Environmental Science & Technology Letters

Letter

Cite This: Environ. Sci. Technol. Lett. 2018, 5, 142−147

pubs.acs.org/journal/estlcu

CO_2 Mineral Sequestration in Naturally Porous Basalt

Wei Xiong,[†] Rachel K. Wells,[‡] Jake A. Horner,[§] Herbert T. Schaef,[§] Philip A. Skemer,[‡] and Daniel E. Giammar*[,†]

[†]Department of Energy, Environmental and Chemical Engineering, Washington University in St. Louis, St. Louis, Missouri 63130, United States

[‡]Department of Earth and Planetary Sciences, Washington University in St. Louis, St. Louis, Missouri 63130, United States

[§]Pacific Northwest National Laboratory, Richland, Washington 99354, United States

Supporting Information

ABSTRACT: Continental flood basalts are extensive geologic features currently being evaluated as reservoirs that are suitable for long-term storage of carbon emissions. Favorable attributes of these formations for containment of injected carbon dioxide (CO_2) include high mineral trapping capacity, unique structural features, and enormous volumes. We experimentally investigated mineral carbonation in whole core samples retrieved from the Grand Ronde basalt, the same formation into which ∼1000 t of CO_2 was recently injected in an eastern Washington pilot-scale demonstration. The rate and extent of carbonate mineral formation at 100 °C and 100 bar were tracked via time-resolved sampling of bench-scale experiments. Basalt cores were recovered from the reactor after 6, 20, and 40 weeks, and three-dimensional X-ray tomographic imaging of these cores detected carbonate mineral formation in the fracture network within 20 weeks. Under these conditions, a carbon mineral trapping rate of 1.24 ± 0.52 kg of CO_2/m^3 of basalt per year was estimated, which is orders of magnitude faster than rates for deep sandstone reservoirs. On the basis of these calculations and under certain assumptions, available pore space within the Grand Ronde basalt formation would completely carbonate in ∼40 years, resulting in solid mineral trapping of ∼47 kg of CO_2/m^3 of basalt.

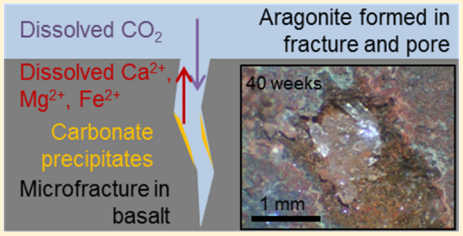

INTRODUCTION

Geologic carbon sequestration is an effective way to mitigate environmental problems caused by anthropogenic CO_2 emissions to the atmosphere.[1,2] It involves injecting CO_2 into deep geologic formations such as sandstone, saline aquifers, and basalt. Sandstone aquifers have a high porosity for physical storage of CO_2 but very limited mineral trapping capacity because of the lack of divalent cations for carbonation reactions.[3] Basalt is an Fe- and Mg-rich (mafic) rock type that has a large mineral trapping capacity to convert CO_2 into solid carbonate minerals.[4,5] CO_2 mineral trapping in basalt reservoirs can occur on time scales of ≤2 years as compared to hundreds or thousands of years in sandstone.[6] In the pilot-scale injection of CO_2 into basalt in Iceland, 95% of injected CO_2 mineralized to calcite within 2 years.[7] In a pilot-scale injection into a basalt formation near Wallula, Washington, mineralization of injected CO_2 to ankerite nodules was observed via 2 year postinjection monitoring.[8]

The dissolution of basalt provides divalent cations Ca^{2+}, Mg^{2+}, and Fe^{2+}, which react with carbonate ions from dissolved CO_2 to form carbonate minerals. Common divalent cation sources are silicate minerals in basalt such as olivine, pyroxene, plagioclase, and glass.[3] Carbonate formation primarily occurs in pores and fractures where transport is controlled by diffusion.[9,10] The diffusion-limited transport in microfractures and pores allows cations to accumulate and reach supersaturation with respect to carbonate minerals.

Prior to our work, there was no bench-scale study of intact basalt rocks that could enable quantitative determination of carbon trapping rates and capacities in these closed systems. The pilot-scale injections are open systems, which makes it difficult to estimate the trapping capacity of the field sites. Most previous laboratory studies of carbon sequestration with basalts investigated carbonation on the surfaces of basalt powders and grains.[11−16] Experiments with basalt rock cores in flow-through systems focused on dissolution[17] and permeability change.[18] X-ray computed tomography (CT) was used for pre-reaction characterization of basalt cores to quantify pore microstructure and specific surface area.[19] Previous work estimated basalt reservoir mineral trapping capacity based on data from field work and geology data, but those studies did not provide estimates of mineral carbonation rates.[20,21]

We investigated carbonate mineral formation in porous Grand Ronde basalt cores with engineered dead-end 100 μm fractures that reacted in water equilibrated with 100 bar of CO_2 at 100 °C for 6, 20, and 40 weeks. The objectives of this work were to quantify the rate of mineral trapping of CO_2 in Grand Ronde basalt via pre- and postreaction CT scanning, to determine the location of carbonate minerals in the pore and

Received: January 29, 2018
Revised: February 22, 2018
Accepted: February 26, 2018
Published: February 27, 2018

DOI: 10.1021/acs.estlett.8b00047
Environ. Sci. Technol. Lett. 2018, 5, 142−147

fracture structure, and to identify the carbonate formation type. This work shows the possibility of quantifying carbonate mineral formation by CT and time-resolved bench-scale experiments, which fills a gap between simulations and large-scale field studies of geological carbon sequestration.

MATERIALS AND METHODS

Materials. A large core sample extracted from a 1022.3–1022.6 m depth of the Grand Ronde formation, which is similar to the formation into which CO_2 was injected near Wallula, was obtained from the DC-6 well in the Hanford archives at Pacific Northwest National Laboratory. The basalt core is porous and contains many millimeter- to centimeter-scale vesicles. The pores are residual gas bubbles that were present during basalt formation. Some millimeter-scale pores are individually located in the cores. These pores may be connected by microsized fractures. The mineral composition of the sample, based on energy and wavelength dispersive spectroscopy analysis, is listed in Table 1; more detailed information can be found in a published open-access report.[22] The basalt is Ca-rich and contains almost no olivine.

Table 1. Grand Ronde Basalt Sample Composition

mineral	composition (vol %)	formula
plagioclase	58	$Ca_{0.51}Na_{0.46}K_{0.03}Al_{1.47}Si_{2.49}O_8$
pyroxene	14	$Mg_{0.72}Fe_{0.59}Ca_{0.60}Si_{1.90}Al_{0.12}O_6$
ilmenite	3	$FeTiO_3$
glass	25	$Si_{0.98}Al_{0.02}Na_{0.008}K_{0.002}Ca_{0.002}Fe_{0.001}O_2$

The large core sample was drilled and cut to make multiple 40 mm long cores with 25.4 mm diameters. Each of these smaller cores was cut into a half-cylinder. The vertical face of one half-core was milled with a 100 μm deep and 11 mm wide straight groove pattern (Figure S1) using a milling machine (Roland model MDX-40a) with a 0.5 mm diamond bur. The groove depth was determined by comparing the z-values of the spots on the groove and the spots on the closest polished surface in an optical microscope (ZEISS, Observer Z1). The half-cores were cleaned using acetone to remove residual chemicals from the cutting process and then sonicated twice in deionized water for 5 min each to remove acetone and any fine-grained material generated during the cutting process. The two half-cylinders were then attached together and coated with epoxy (MasterBond EP42HT-2) on the side and bottom surfaces, exposing only the top surface with the fracture inlet. In this way, a microfracture was created in the middle of the core to mimic a dead-end fracture in bulk basalt that is exposed to the reactive solution.

Static Batch Experiment. Three of the epoxy-coated fractured basalt cores were placed in a PTFE (polytetrafluoroethylene) sample holder, which sat in a PTFE liner inside of a 600 mL stainless steel high-pressure vessel (Parr Instrument). A volume of 192 mL (64 mL per core) of deionized water was added to fully immerse the cores (Figure S2), and the reactor was heated to 100 °C. The water:rock mass ratio was 1.8:1. The headspace was pressurized to 100 bar of CO_2 and maintained during the experiment with a syringe pump (500D, Teledyne Isco). The cores were collected one by one after reaction for 6, 20, and 40 weeks after depressurization and cooling to room conditions. Residual solution on the collected cores was first absorbed by tissues. This left minimal amounts of solution to be air-dried and minimized any evaporation-induced precipitation. At each sampling time, 64 mL of solution was removed to maintain the same solid:water ratio in the reactor. Liquid samples were taken from the solution and filtered with 0.2 μm filters after a core sample was collected. Liquid samples were immediately acidified with HNO_3. The liquid samples taken after degassing may differ from the composition under high temperatures and pressures. Cooling and depressurizing can cause carbonate minerals to form. Calculations using Geochemist's Workbench 10.0 (Supporting Information) show that precipitation inside the microfracture due to the sampling process is negligible and that the bulk solution would have

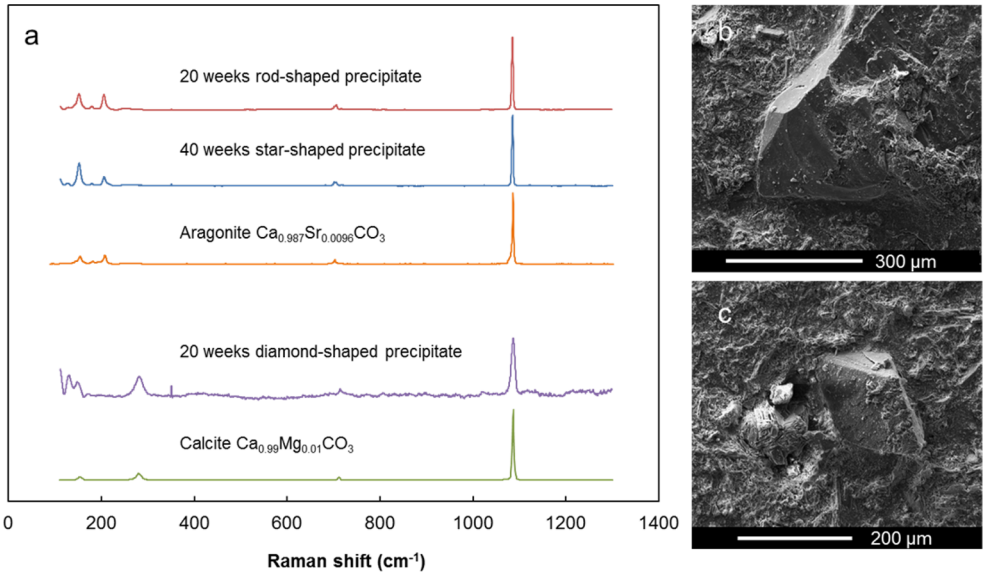

Figure 1. (a) Raman spectra of the precipitates formed in basalt with aragonite (R150021) and calcite (R040070) standards from the RRUFF database. (b) SEM image of the end of a millimeter-scale rod-shaped precipitate in a basalt core reacted for 20 weeks. (c) SEM image of a micrometer-scale diamond-shaped precipitate. SEM–EDS spectra for precipitates shown in panels b and c are shown in Figure S5. The XRD result for the rod-shape precipitates is shown in Figure S6.

DOI: 10.1021/acs.estlett.8b00047
Environ. Sci. Technol. Lett. 2018, 5, 142–147

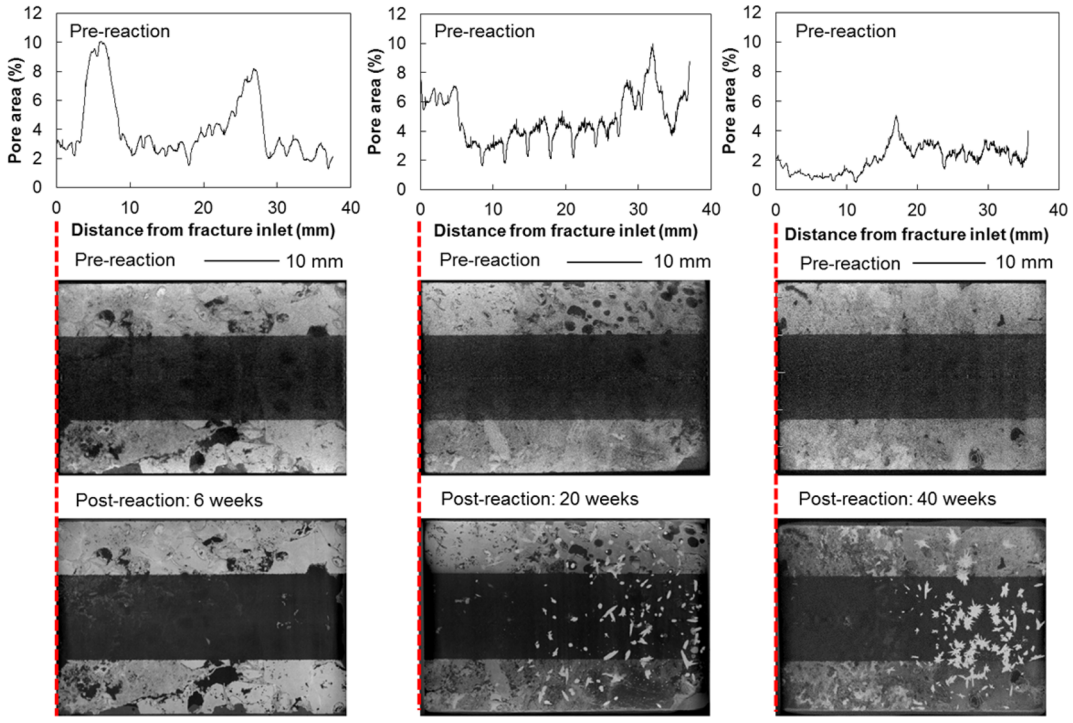

Figure 2. Pore area percentages of the core cross section and pre- and postreaction CT images. The entire core porosity based on CT segmentation was 4.04, 4.83, and 2.09% for the pre-reaction 6, 20, and 40 week cores, respectively. The red dashed lines indicate the fracture inlet. Movies of the three-dimensional (3D) CT images are available in the Supporting Information.

some precipitation induced by the cooling and depressurization process. To minimize the influence of the process of cooling and depressurizing for sample collection and restarting the batch, the overall process was completed within 5 h. Before being heated and pressurized, the vessel was flushed three times with 10 bar of CO_2 to remove residual O_2.

Analytical Methods. The three basalt cores were scanned by X-ray computed tomography (CT) before (Scanco uCT 40) and after reaction (Nikon Metrology XTH225, Zeiss Xradia Versa 520). The voxel resolution of the CT images was 15 μm for the pre-reaction cores, 22.5 μm for the 6 and 20 week samples, and 15.5 μm for the 40 week sample. The precipitate volume was assessed by CT segmentation using ORS Visual. The pore area percentage on each CT slice was calculated in ImageJ using the Zen threshold. After CT scans were collected, the cores were cut open. Optical microscopy (LEICA, DFC295) was used to detect precipitates along the fracture surface, and Raman spectra of precipitates were recorded (HoloLab Series 5000 Laser Raman Microprobe, Kaiser Optical). The spectra were compared with standards from the RRUFF database for mineral identification. The micro-X-ray diffraction analysis was conducted on a finely crushed secondary precipitate that was removed from the reacted core. The powdered sample was placed into a glass capillary tube (Charles Supper Co.) for analysis on a D8 Discover X-ray diffractometer (Bruker AXS). The morphology and elemental composition of the precipitate were examined by scanning electron microscopy and energy dispersive X-ray spectroscopy (SEM–EDS) (FEI Nova 230). Aqueous samples were analyzed by inductively coupled plasma mass spectrometry (PerkinElmer, Elan DRC II) and ion chromatography (Thermo Scientific, DIONEX ICS-1600). The pH was calculated on the basis of charge balance for the solution with measured dissolved species and dissolved CO_2 calculated using a previous model.[23] Saturation indices of secondary precipitates in the bulk solution after reaction were calculated using SpecE8 in Geochemist's Workbench with measured dissolved species and the default database.

RESULTS AND DISCUSSION

Calcium Carbonate Formation. The carbonation products are calcium carbonates. The millimeter-scale rod- and star-shaped precipitates (Figure 1b and Figures S3 and S4) formed in the 20 and 40 week samples were aragonite as identified by Raman spectroscopy (Figure 1a) and micro-XRD (Figure S5). Trace amounts of micrometer-scale diamond-shaped precipitates (Figure 1c and Figures S3 and S4) were identified as calcite by Raman spectroscopy. The formation of aragonite versus calcite is affected by both temperature and the Mg:Ca ratio in the solution.[24] Calcite is more likely to form in cold water at lower Mg:Ca ratios.[25] A previous study showed that calcite could form initially and then aragonite began to nucleate and grow because the Mg:Ca ratio in the solution increased as precipitation proceeded.[24] Ankerite [$Ca(Fe,Mg,Mn)(CO_3)_2$] was observed in the pilot-scale field study.[8] In the field injection, the temperature was 36–44 °C and the pressure was ~77 bar.[8] In our previous experiment using Columbia River Flood basalt, siderite was observed as the predominant carbonation product in a fracture,[26,27] but that basalt was much richer in iron than the Grand Ronde basalt. Reaction path modeling based on the fluid data from the CarbFix project indicates siderite forms at pH <5 and calcite forms at higher pHs.[28] During the reaction, the pH inside the basalt fracture and pores could be high enough for calcium carbonate formation.

Other secondary minerals such as iron oxides were observed in our previous work with other basalts,[10,26] but we did not observe them in this study, which may be due to the relatively

DOI: 10.1021/acs.estlett.8b00047
Environ. Sci. Technol. Lett. 2018, 5, 142–147

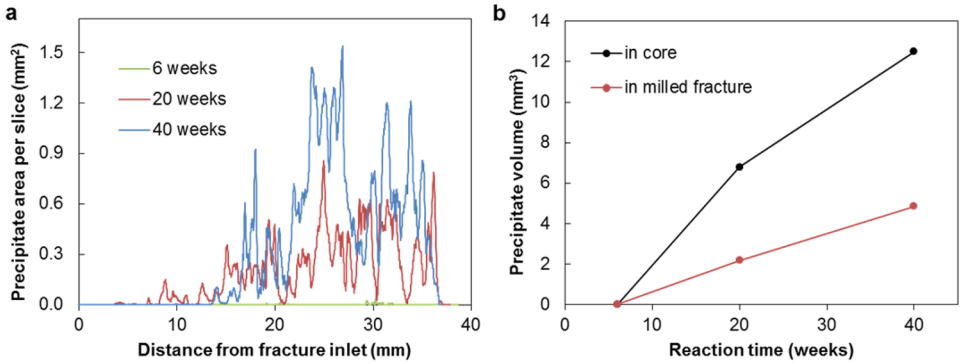

Figure 3. (a) Precipitate area in each round cross section CT slice from segmentation. (b) Total precipitate volume in the entire core and in the 100 μm fracture.

low Fe content of the Grand Ronde basalt. Some Si-rich secondary precipitates were observed on the surface of carbonate minerals (Figure S4c).

Bulk solution chemistry provides information about basalt dissolution. The dissolved species in the bulk solution were from the exposed top surface and the diffusion from the fracture. Ca^{2+} has the highest measured concentration among divalent cations in the bulk solution (Figure S6). It is possible that some of the dissolved Fe^{2+} reacted with residual O_2 in the system to generate Fe^{3+} that then precipitated in iron oxides. The concentrations of Cl^- and SO_4^{2-} were probably from evaporated residual brine left inside the porous basalt. The high concentration of Na^+ probably results from this residual brine and the dissolution of plagioclase. The calculated pH in the bulk solution was 5.1−5.4 (Figure S7). The calculated saturation indices (Figure S8) determined based on the measured concentrations and calculated dissolved CO_2 indicate that chalcedony (SiO_2) and multiple carbonate minerals could precipitate. However, the formation of carbonate minerals depends on not only supersaturation status but also the kinetics of nucleating and growing a particular precipitate. Carbonate minerals were rarely found in solution after cooling and depressurization, indicating that the bulk solution was usually far from equilibrium status to form precipitates during the sampling process (calculations in the Supporting Information). The analysis of the bulk solution provides insights into the solution chemistry inside the microfracture, which could not be directly sampled or examined.

The carbonate minerals that formed represented their presence at the reactor temperature and pressure and were not induced by the degassing and cooling processes for sampling because (a) their levels continued to increase with reaction time, (b) a previous study with the same approach found good agreement between experimental data and a model that assumed constant pressure and temperature,[26] (c) the calcium carbonate crystals were too well-developed to have formed from a rapid degassing event, and (d) a simplified reaction path model (Supporting Information) shows negligible changes in the amount of precipitate inside the microfracture with a change in temperature and pressure.

Location of Carbonate Minerals. Carbonate minerals mostly formed along the fracture, although the entire basalt core was porous (Figures 2 and 3D, illustrations in Figures S9 and S10, and Movies S1 and S2). The fracture, which was the main transport pathway from the bulk solution, represented only 0.2% of the core volume (with a 3.65% average porosity). However, after reaction for 40 weeks, carbonate precipitates were also found in distant pores that had no obvious connection with the fracture (Movie S1 and Figure S11). Carbonate precipitates were observed in the pores that were directly connected to the fracture (Movie S2, 20 week sample). This observation indicates that dissolved CO_2 can migrate into the inner porous Grand Ronde basalt body and that carbonation reactions could happen throughout the entire pore space of the rock.

The spatially localized formation of carbonate minerals within the fracture was a result of opposing chemical gradients from the fracture inlet to the dead end.[9,10,29] The bulk solution was rich in dissolved CO_2 but contained very limited cations for carbonate precipitation. The fractured porous basalt core initially had no dissolved CO_2, and dissolved CO_2 diffused into the core along the microfracture. As the reaction progressed, cations such as Ca^{2+} were released from minerals in the basalt to the solution in the fracture and pores. Cations diffused out of the fracture to the bulk solution. Localized cation concentrations along the fracture are determined by both diffusive transport and dissolution/precipitation reactions. Cation concentrations should be lower near the fracture inlet, which contacted the bulk solution. Regions away from the fracture inlet would contain higher cation concentrations and could be more favorable for carbonate minerals to precipitate.

Carbonation Rate. The precipitate area per CT slice shows an uneven distribution of carbonate minerals with distance from the fracture inlet (Figure 3a). Carbonate precipitates may potentially plug the pores and passivate the reaction process; however, the formation of carbonate minerals did not block the transport pathways into deeper zones within the reaction time in this study.

The precipitate volume was obtained from CT segmentation (Figure 3b). On the basis of the CT resolution, four or five vertical slices were selected across the 100 μm fracture. The precipitate volume in these slices was considered "in milled fracture". The precipitate volume in the entire core, including the fracture and pre-existing pores, was considered "in core". The difference between these two precipitate volumes is the amount of precipitate that occurred in pores that are separate from the 100 μm fracture. As the reaction continued, more carbonate minerals formed in these pores (Figure 3b). Approximately 13% of the milled fracture volume was occupied with carbonate precipitates after 40 weeks, leaving ample volume for future reactions.

Carbonate minerals formed, and then their volume increased over the course of the 40 week experiment. The first 6 weeks in which carbonates did not form may have been needed for the

DOI: 10.1021/acs.estlett.8b00047
Environ. Sci. Technol. Lett. 2018, 5, 142−147

solution to become sufficiently supersaturated to overcome the nucleation barrier. After nucleation occurred, carbonate growth was almost linear. By fitting the three data points ("in core" data in Figure 3b) to a line, we determined the carbonation rate as the slope. The calculated rate is 1.24 ± 0.52 kg of CO_2/m^3 of basalt per year or 958 ± 400 cm^3 of $CaCO_3/m^3$ of basalt per year with a 95% confidence level, assuming that all precipitates are aragonite.

Mineral Trapping Capacity and Time. The average porosity of the three cores before reaction was 3.65% from CT segmentation results. Assuming CO_2 can be fixed as aragonite (2.93 g/cm^3 or as 1.29 g of CO_2/cm^3) in all available pore space (36500 cm^3/m^3), then the total mineral trapping capacity of the Grand Ronde basalt is 47 kg of CO_2/m^3 of basalt. The Iceland Geosurvey showed that 70−130 kg of CO_2 can be stored in 1 m^3 of basaltic rock that had naturally come in contact with CO_2,[30] a number comparable to that observed in this study for the Grand Ronde basalt. For sandstone with 10−40% porosity, the CO_2 storage capacity as a buoyant phase is 19−75 kg of CO_2/m^3 of sandstone at 100 °C and 100 bar. This value is comparable to that achieved with mineral trapping with the Grand Ronde basalt, but the CO_2 remains as a buoyant phase and not as the stable carbonate minerals in the basalt. In the pilot-scale injection in Washington, 1000 t of CO_2 was injected into a 59 m thick Grand Ronde basalt formation layer (828−887 m depth).[8] For the carbonate trapping capacity determined in this study, it would take a volume of 21200 m^3 of basalt to mineralize all of the injected CO_2. This would be a cylinder with a radius of only 11 m if the full layer thickness were available. In an ideal scenario, if the carbonation rate were to remain constant (1.24 kg of CO_2/m^3 of basalt per year) and the porosity were 3.65%, then it would take 38 years to completely fill the pore space at 100 °C in the Grand Ronde basalt.

CO_2 mineral trapping is much more rapid in basalt than in sandstone reservoirs. In sandstone reservoirs, supercritical CO_2 can be stored in a buoyant phase for hundreds to thousands of years before mineral trapping happens.[1] A simulation of carbon sequestration in a glauconitic sandstone aquifer calculated that 17 kg of CO_2/m^3 would be trapped in mineral phases after 100000 years.[31] If the mineralogy of Gulf Coast sediments is used in the simulation, the mineral trapping could reach 90 kg of CO_2/m^3 of sediments after 100000 years.[31]

Environmental Implications. We confirmed that carbonate minerals can form within weeks of injection of CO_2 into fractured and porous basalt. The formation of carbonate minerals is unevenly distributed in zones for which solute transport is controlled by diffusion. In the fractured Grand Ronde basalt, the formation of carbonate did not block transport pathways or inhibit reactions within the 40 week experimental time of this study. This study demonstrated the possibility of estimating the mineral trapping capacity of basalts and carbonation rate by time-resolved bench-scale experiments. The mineral trapping rate and capacity of porous basalt are much greater than those of sandstone reservoirs. However, at actual field sites, diffusion and pore clogging due to precipitation over times longer than those examined in this study may slow the rate of mineral trapping for carbon sequestration. Future study using bench-scale experiments to obtain the carbonation rate and mineral trapping capacity should consider longer reaction times and can be integrated with reactive transport modeling.

■ ASSOCIATED CONTENT

Supporting Information

The Supporting Information is available free of charge on the ACS Publications website at DOI: 10.1021/acs.estlett.8b00047.

Schematics of the fractured core and batch reactor, CT images, optical microscopic images, SEM−EDX and XRD of precipitates, bulk solution species concentrations, pH and saturation index calculations, and reaction path modeling (PDF)
Movie S1 (AVI)
Movie S2 (AVI)

■ AUTHOR INFORMATION

Corresponding Author

*Campus Box 1180, One Brookings Drive, St. Louis, MO 63130. Phone: 314-935-6849. Fax: 314-935-7211. E-mail: giammar@wustl.edu.

ORCID

Herbert T. Schaef: 0000-0002-4546-3979
Daniel E. Giammar: 0000-0002-4634-5640

Notes

The authors declare no competing financial interest.

■ ACKNOWLEDGMENTS

This work was funded by the U.S. Department of Energy (DE-FE0023382). The authors thank Professor Jill Pasteris for her help with Raman spectroscopy and Dr. Hélène Couvy for assistance with core preparation. Daniel Leib and Professor James Fitzpatrick enabled our use of X-ray computed tomography. Professor Brian Ellis and Anne Menefee provided constructive comments on the overall project.

■ REFERENCES

(1) IPCC Special Report on Carbon Dioxide Capture and Storage. Technical Report; Cambridge University Press for the Intergovernmental Panel on Climate Change: Cambridge, U.K., 2005.

(2) Giammar, D. E.; Bruant, R. G.; Peters, C. A. Forsterite dissolution and magnesite precipitation at conditions relevant for deep saline aquifer storage and sequestration of carbon dioxide. *Chem. Geol.* **2005**, *217*, 257−276.

(3) Oelkers, E. H.; Gislason, S. R.; Matter, J. Mineral Carbonation of CO_2. *Elements* **2008**, *4*, 333−337.

(4) Goff, F.; Lackner, K. Carbon dioxide sequestering using ultramafic rocks. *Environ. Geosci.* **1998**, *5*, 89−101.

(5) Matter, J. M.; Kelemen, P. B. Permanent storage of carbon dioxide in geological reservoirs by mineral carbonation. *Nat. Geosci.* **2009**, *2*, 837−841.

(6) Snæbjörnsdóttir, S. Ó.; Oelkers, E. H.; Mesfin, K.; Aradóttir, E. S.; Dideriksen, K.; Gunnarsson, I.; Gunnlaugsson, E.; Matter, J. M.; Stute, M.; Gislason, S. R. The chemistry and saturation states of subsurface fluids during the in situ mineralisation of CO_2 and H_2S at the CarbFix site in SW-Iceland. *Int. J. Greenhouse Gas Control* **2017**, *58*, 87−102.

(7) Matter, J. M.; Stute, M.; Snaebjornsdottir, S. O.; Oelkers, E. H.; Gislason, S. R.; Aradottir, E. S.; Sigfusson, B.; Gunnarsson, I.; Sigurdardottir, H.; Gunnlaugsson, E.; Axelsson, G.; Alfredsson, H. A.; Wolff-Boenisch, D.; Mesfin, K.; Taya, D. F. D.; Hall, J.; Dideriksen, K.; Broecker, W. S. Rapid carbon mineralization for permanent disposal of anthropogenic carbon dioxide emissions. *Science* **2016**, *352*, 1312−1314.

(8) McGrail, B. P.; Schaef, H. T.; Spane, F. A.; Cliff, J. B.; Qafoku, O.; Horner, J. A.; Thompson, C. J.; Owen, A. T.; Sullivan, C. E. Field Validation of Supercritical CO_2 Reactivity with Basalts. *Environ. Sci. Technol. Lett.* **2017**, *4*, 6−10.

DOI: 10.1021/acs.estlett.8b00047
Environ. Sci. Technol. Lett. 2018, 5, 142−147

(9) Giammar, D. E.; Wang, F.; Guo, B.; Surface, J. A.; Peters, C. A.; Conradi, M. S.; Hayes, S. E. Impacts of Diffusive Transport on Carbonate Mineral Formation from Magnesium Silicate-CO_2-Water Reactions. *Environ. Sci. Technol.* **2014**, *48*, 14344−14351.
(10) Xiong, W.; Wells, R. K.; Giammar, D. E. Carbon Sequestration in Olivine and Basalt Powder Packed Beds. *Environ. Sci. Technol.* **2017**, *51*, 2105−2112.
(11) Gysi, A. P.; Stefansson, A. CO_2-water-basalt interaction. Low temperature experiments and implications for CO_2 sequestration into basalts. *Geochim. Cosmochim. Acta* **2012**, *81*, 129−152.
(12) Rosenbauer, R. J.; Thomas, B.; Bischoff, J. L.; Palandri, J. Carbon sequestration via reaction with basaltic rocks: Geochemical modeling and experimental results. *Geochim. Cosmochim. Acta* **2012**, *89*, 116−133.
(13) Galeczka, I.; Wolff-Boenisch, D.; Oelkers, E. H.; Gislason, S. R. An experimental study of basaltic glass−H_2O−CO_2 interaction at 22 and 50°C: implications for subsurface storage of CO_2. *Geochim. Cosmochim. Acta* **2014**, *126*, 123−145.
(14) Schaef, H. T.; Horner, J. A.; Owen, A. T.; Thompson, C. J.; Loring, J. S.; McGrail, B. P. Mineralization of Basalts in the CO_2-H_2O-SO_2-O_2 System. *Environ. Sci. Technol.* **2014**, *48*, 5298−5305.
(15) Hellevang, H.; Haile, B. G.; Tetteh, A. Experimental study to better understand factors affecting the CO_2 mineral trapping potential of basalt. *Greenhouse Gases: Sci. Technol.* **2017**, *7*, 143−157.
(16) Wolff-Boenisch, D.; Galeczka, I. Flow-through reactor experiments on basalt-(sea) water-CO_2 reactions at 90°C and neutral pH. What happens to the basalt pore space under post-injection conditions? *Int. J. Greenhouse Gas Control* **2018**, *68*, 176−190.
(17) Luhmann, A. J.; Tutolo, B. M.; Tan, C.; Moskowitz, B. M.; Saar, M. O.; Seyfried, W. E. Whole rock basalt alteration from CO_2-rich brine during flow-through experiments at 150° C and 150bar. *Chem. Geol.* **2017**, *453*, 92−110.
(18) Luhmann, A. J.; Tutolo, B. M.; Bagley, B. C.; Mildner, D. F.; Seyfried, W. E.; Saar, M. O. Permeability, porosity, and mineral surface area changes in basalt cores induced by reactive transport of CO_2-rich brine. *Water Resour. Res.* **2017**, *53*, 1908−1927.
(19) Kanakiya, S.; Adam, L.; Esteban, L.; Rowe, M.; Shane, P. Dissolution and secondary mineral precipitation in basalts due to reactions with carbonic acid. *Journal of Geophysical Research: Solid Earth* **2017**, *122*, 4312−4327.
(20) Goldberg, D. S.; Takahashi, T.; Slagle, A. L. Carbon dioxide sequestration in deep-sea basalt. *Proc. Natl. Acad. Sci. U. S. A.* **2008**, *105*, 9920−9925.
(21) Gislason, S. R.; Wolff-Boenisch, D.; Stefansson, A.; Oelkers, E. H.; Gunnlaugsson, E.; Sigurdardottir, H.; Sigfusson, B.; Broecker, W. S.; Matter, J. M.; Stute, M.; Axelsson, G.; Fridriksson, T. Mineral sequestration of carbon dioxide in basalt: A pre-injection overview of the CarbFix project. *Int. J. Greenhouse Gas Control* **2010**, *4*, 537−545.
(22) Wells, R.; Giammar, D.; Skemer, P. Sample Library of Natural and Artificial Basalts. https://edx.netl.doe.gov/dataset/sample-library-of-natural-and-artificial-basalts, 2016 (accessed February 23, 2018).
(23) Duan, Z. H.; Sun, R. An improved model calculating CO_2 solubility in pure water and aqueous NaCl solutions from 273 to 533 K and from 0 to 2000 bar. *Chem. Geol.* **2003**, *193*, 257−271.
(24) Morse, J. W.; Arvidson, R. S.; Luttge, A. Calcium carbonate formation and dissolution. *Chem. Rev.* **2007**, *107*, 342−381.
(25) Morse, J. W.; Wang, Q.; Tsio, M. Y. Influences of temperature and Mg: Ca ratio on $CaCO_3$ precipitates from seawater. *Geology* **1997**, *25*, 85−87.
(26) Xiong, W.; Wells, R. K.; Menefee, A. H.; Skemer, P.; Ellis, B. R.; Giammar, D. E. CO_2 mineral trapping in fractured basalt. *Int. J. Greenhouse Gas Control* **2017**, *66*, 204−217.
(27) Adeoye, J. T.; Menefee, A. H.; Xiong, W.; Wells, R. K.; Skemer, P.; Giammar, D. E.; Ellis, B. R. Effect of transport limitations and fluid properties on reaction products in fractures of unaltered and serpentinized basalt exposed to high PCO2 fluids. *Int. J. Greenhouse Gas Control* **2017**, *63*, 310−320.
(28) Snæbjörnsdóttir, S. Ó.; Gislason, S. R.; Galeczka, I. M.; Oelkers, E. H. Reaction path modelling of in-situ mineralisation of CO2 at the CarbFix site at Hellisheidi, SW-Iceland. *Geochim. Cosmochim. Acta* **2018**, *220*, 348−366.
(29) Xiong, W.; Giammar, D. Forsterite Carbonation in Zones with Transport Limited by Diffusion. *Environ. Sci. Technol. Lett.* **2014**, *1*, 333−338.
(30) Wiese, F.; Fridriksson, T.; Ármannsson, H. Iceland Geosurvey. www.os.is/gogn/Skyrslur/ISOR-2008/ISOR-2008-003.pdf, 2008 (accessed February 23, 2018).
(31) Xu, T. F.; Apps, J. A.; Pruess, K. Numerical simulation of CO_2 disposal by mineral trapping in deep aquifers. *Appl. Geochem.* **2004**, *19*, 917−936.

DOI: 10.1021/acs.estlett.8b00047
Environ. Sci. Technol. Lett. 2018, 5, 142−147